Practical Solutions to Polarization-Mode-Dispersion Emulation and Compensation

Lianshan Yan, *Senior Member, IEEE*, *Member, OSA*, X. Steve Yao, *Member, IEEE*, *Member, OSA*, M. C. Hauer, *Student Member, IEEE*, *Student Member, OSA*, and A. E. Willner, *Fellow, IEEE*, *Fellow, OSA*

Invited Paper

***Abstract*—Polarization-mode dispersion (PMD) still remains a challenge for high-data-rate optical-communication systems. Practical solutions are desirable for PMD emulation, monitoring, and compensation. The authors review and compare various techniques for PMD emulation and compensation, with an emphasis on the application of programmable differential-group-delay (DGD) elements for manipulating PMD effects. The authors pay special attention to advanced emulation techniques, such as importance sampling and the hinge model, for practical applications. The tunability of programmable DGD elements proves to be attractive for both system performance evaluation and overall optimization.**

***Index Terms*—Differential group delay (DGD), importance sampling (IS), optical communications, polarization mode dispersion (PMD).**

I. Introduction

THE CONTINUOUS need for greater bandwidth and capacity to support existing and emerging technologies, such as fiber-to-the-home (FTTH) and Internet Protocol Television (IPTV), drive optical-communication systems to higher and higher data rates per wavelength channel, from 10 to 40, 160, and now even 640 Gb/s [1]. Degrading effects that tended to cause noncatastrophic events at lower bit rates have become critical concerns for high-performance networks. Among them, polarization-mode dispersion (PMD) is perhaps the largest concern and, therefore, has garnered a great amount of attention [2]–[4].

The PMD arises in an optical fiber from asymmetries in the fiber core that induce a small amount of birefringence that randomly varies along the length of the fiber. This birefringence causes the power in each optical pulse to split between the two polarization modes of the fiber and travel at different speeds, creating a differential group delay (DGD) between the two modes that can result in pulse spreading and intersymbol interference. PMD becomes a unique and challenging hurdle for high-performance systems mainly due to its dynamic and random nature. The polarization state is generally unknown and wanders with time. In general, PMD effects are wavelength (channel) dependent and can vary over a time scale of milliseconds [5], [6]. As a random variable, the DGD follows a Maxwellian distribution for which high-DGD points in the tail of the distribution can lead to network outages. Typically, system designers require the outage probability for high-performance networks to be 10^{-6} or less (penalty > 1 dB for < 1 min/yr) [2].

Clearly, the most straightforward approach to overcoming the effects of PMD is to employ newly manufactured low-PMD optical fibers, which have PMD values < 0.1 ps/km$^{1/2}$ [7]. However, much of the previously embedded fiber has high PMD values between 0.5 and 1.0 ps/km$^{1/2}$ or even higher. The reality of deploying new systems over the embedded fiber means that the PMD monitoring and compensation are important for PMD mitigation. Unlike other degrading effects such as chromatic dispersion, the PMD is a time-varying random process making emulation difficult, but it is still crucial to system testing.

PMD emulation is important for two key reasons. First, network designers need to test and verify new technologies in the presence of PMD, especially for systems that will not deploy PMD compensators. It is not feasible to perform a system evaluation using the embedded fiber links without data traffic interruption. Second, it is impossible to rapidly explore a large number of different fiber ensembles using the optical fiber itself, a general requirement for determining PMD-induced penalty distributions and outages.

In this paper, we will review key techniques for generating first-order and higher order PMD effects, with an emphasis on the advanced emulation techniques using programmable DGD elements. These elements have become practical and flexible tools that can be implemented in several different PMD emulation and compensation techniques. The advantages and limitations of such applications are discussed, as well as insights into which solutions are most practical from the authors' perspectives.

This paper is structured as follows: A review of PMD emulator theory and common implementations is presented in Section II. Programmable DGD elements are introduced in Section III with a description of how they are applied to emulators with tunable PMD statistics. Their application to advanced PMD emulation techniques is covered in Section IV. The PMD compensation related techniques are discussed in Section V, followed by a discussion of practical PMD issues in Section VI.

Manuscript received April 11, 2006; revised July 13, 2006.

L. Yan and X. S. Yao are with the General Photonics Corporation, Chino, CA 91710 USA (e-mail: lsyan@generalphotonics.com).

M. C. Hauer and A. E. Willner are with the Department of Electrical Engineering—Systems, University of Southern California, Los Angeles, CA 90089-2565 USA.

Digital Object Identifier 10.1109/JLT.2006.883610

II. PMD Emulation

Generally, a PMD emulator can be formed by a concatenation of individual sections of the PMD; therefore, before comparing various PMD emulation techniques, a brief review of the PMD concatenation equations and recursion relation often used to model PMD emulators in Stokes space is helpful and, henceforth, presented. Further details can be found in the literature [2], [8]–[10].

The PMD of a fiber is represented as a three-dimensional vector $\mathbf{\Omega}$ on the Poincaré sphere and is typically defined by the key equation

$$\frac{d\mathbf{s}}{d\omega} = \mathbf{\Omega} \times \mathbf{s} \tag{1}$$

that relates the rate of change with frequency of the input or output state of polarization (SOP) $\mathbf{s}$ to the PMD vector. The magnitude of $\mathbf{\Omega}$ corresponds to the DGD ($\Delta\tau$) of the fiber. For an emulator comprising multiple linear birefringent sections, the PMD vector at the output of section $n+1$ can be determined using the following recursion relation:

$$\mathbf{\Omega}_{n+1} = \mathbf{\Delta\Omega}_{n+1} + \mathbf{B\Omega}_n \tag{2}$$

where $\mathbf{\Omega}_n$ is the PMD vector of the previous n sections, $\mathbf{\Delta\Omega}_{n+1} = (\Delta\tau_{n+1}, 0, 0)$ is the PMD vector of section $n+1$, and $\mathbf{B}$ is the 3×3 Müller matrix that transforms the polarization state from the input to the output of section $n+1$. Similarly, the recursion relation used to compute the second-order PMD (SOPMD), assuming no frequency dependence of the PMD vector for individual sections, is

$$\mathbf{\Omega}_{\omega}^{n+1} = \mathbf{B\Omega}_{\omega}^{n} + \mathbf{\Delta\Omega}_{n+1} \times (\mathbf{B\Omega}_n). \tag{3}$$

For emulators with rotatable sections or tunable birefringence, the transfer matrix $\mathbf{B}$ for each birefringent section can be expressed as a product of the rotation matrix $\mathbf{R}_{\mathrm{z}}$ and the propagation matrix $\mathbf{R}_{\mathrm{x}}$

$$\mathbf{B} = \mathbf{R}_{\mathrm{x}}\mathbf{R}_{\mathrm{z}} = \begin{bmatrix} \mathbf{0} & -\mathbf{\Omega}_{\mathrm{z}} & \mathbf{\Omega}_{\mathrm{y}} \\ \mathbf{\Omega}_{\mathrm{z}} & \mathbf{0} & -\mathbf{\Omega}_{\mathrm{x}} \\ -\mathbf{\Omega}_{\mathrm{y}} & \mathbf{\Omega}_{\mathrm{x}} & \mathbf{0} \end{bmatrix}. \tag{4}$$

A more general expression of $\mathbf{B}'\mathbf{B}^{-1}$ is listed in [9].

The propagation matrix $\mathbf{R}_{\mathrm{x}}$ is

$$\mathbf{R}_{\mathrm{x}}(\gamma) = \begin{bmatrix} 1 & 0 & 0 \\ 0 & \cos\gamma & -\sin\gamma \\ 0 & \sin\gamma & \cos\gamma \end{bmatrix} \tag{5}$$

where

$$\gamma = \omega \cdot \Delta\tau_n. \tag{6}$$

The phase γ is the birefringence-induced phase retardation between the two polarization modes, ω is the optical carrier frequency, and $\Delta\tau_n$ is the DGD of the nth section.

The form of the rotation matrix $\mathbf{R}_{\mathrm{z}}$ depends on the polarization-coupling configuration between sections. Two widely used models include simple polarization rotators between sections and uniform polarization scattering between sections using polarization controllers. For polarization rotators, $\mathbf{R}_{\mathrm{z}}$ is defined as

$$\mathbf{R}_{\mathrm{z}}(\theta) = \begin{bmatrix} \cos 2\theta & \sin 2\theta & 0 \\ -\sin 2\theta & \cos 2\theta & 0 \\ 0 & 0 & 1 \end{bmatrix} \tag{7}$$

with the physical rotation angle denoted as θ. For random polarization scattering between sections, the rotation matrix can be written as

$$\mathbf{R}_{\mathrm{z}}(\theta, \phi) = \begin{bmatrix} \phi & \sqrt{\mathbf{1}-\phi^2}\cos\theta & \sqrt{\mathbf{1}-\phi^2}\sin\theta \\ \sqrt{\mathbf{1}-\phi^2} & \phi\cos\theta & \phi\sin\theta \\ \mathbf{0} & -\sin\theta & \cos\theta \end{bmatrix} \tag{8}$$

where θ and ϕ are uniformly distributed over [0, 2π] and [−1,1], respectively.

With the appropriate choice of rotation matrix and values for θ, γ, and/or φ, various types of emulators can be modeled. Monte Carlo methods can be used to select random values for the emulator parameters in order to determine the time and frequency statistics of the first-order and higher order PMD components of a given emulator configuration.

In a wavelength-division-multiplexed (WDM) system, the polarization states of different channels with sufficient frequency spacing are generally random and uncorrelated after transmission over an optical fiber with nonnegligible PMD (even if the polarization states are aligned at the transmitter). For example, a fiber with 40 ps of PMD shows a negligible correlation between PMD vectors when the channel spacing is more than 0.2 nm ([2], [11]). For high bandwidth channels, the PMD vectors at different frequencies within the spectrum of an individual channel can become uncorrelated. For PMD emulators, it has been shown that the use of a large number of unequal length (or unequal DGD) sections is necessary to reduce the background frequency autocorrelation of the PMD vector. After the PMD vector has been obtained at several equally spaced frequencies for numerous random states of a PMD emulator (either experimentally or using the equations above), the normalized background autocorrelation function (ACF) can by computed using [9]

$$\mathrm{ACF} = \frac{1}{N_{\mathrm{f}}} \sum_{|\omega_i - \omega_0| > \pi/<\Delta\tau>} \left| \frac{\langle \Omega(\omega_i) \cdot \Omega(\omega_0) \rangle}{\langle \Omega(\omega_0) \cdot \Omega(\omega_0) \rangle} \right| \tag{9}$$

where ω_i represents N_{f} angular frequencies equally spaced outside the bandwidth of the autocorrelation peak centered at ω_0. For emulators that are designed to mimic the statistical behavior of real fibers, the background autocorrelation level should be close to zero.

A. PMD Emulator Categories

The importance of characterizing and compensating for the effects of PMD on various systems has led to the development of numerous techniques for generating PMD in the laboratory [12]–[32]. Over time, it has become clear that different applications or testing phases require different types of PMD emulation. This includes methods for accurately and rapidly

emulating the random variations of the PMD in real fibers as well as techniques for generating specific components and combinations of first-order and higher order PMDs in a predictable and repeatable way. To better organize the field of PMD emulation, researchers have begun to classify these methods into two major categories, PMD emulators and PMD sources.

In a broad sense, devices intended to ***mimic*** the random ***statistical*** behavior of long single-mode fibers (Maxwellian DGD distribution, accurate higher order effects, and correct frequency autocorrelation properties) have been termed as "statistical PMD ***emulators***," "all-order emulators," and, often, just "emulators." Devices that ***map*** the PMD space to the emulator settings and predictably ***generate*** the desired values of first-order and/or higher order PMDs at some wavelength or span of wavelengths are generally termed as "PMD ***sources***," "deterministic emulators," "programmable PMD elements," or "isolated-order emulators" [16].

PMD sources or deterministic emulators enable a tester to quantify the performance of a device or system over a well-defined portion of the PMD sample space and to focus on PMD states that are particularly significant or problematic. This is a crucial requirement for the development of standardized testing methods to enable designers to make apples-to-apples comparisons of transmitter–receiver pairs. In these cases, polarization scrambling is generally required before a PMD source to locate worst case events. Deterministic emulators are usually configured to generate only certain components or combinations of first-order and higher order PMDs in order to isolate the effects due to them [16], [20]–[23]. This level of programmability and repeatability usually comes at the cost of having a limited set of PMD coordinates that can be explored for a given source configuration. Thus, as a final testing stage, it is often necessary and desirable to test a system using an all-order statistical emulator to confirm the system performance under the conditions that closely mimic the full random variations of real fibers.

B. Isolated-Order PMD Emulators

A fixed DGD emulator can be a piece of polarization-maintaining fiber (PMF) or a birefringent crystal. Such emulators have limited use in terms of emulating PMD effects, and are more often used in PMD compensation schemes. On the contrary, a tunable DGD emulator has multiple applications including 1) generating programmable DGD distributions (Maxwellian or otherwise), 2) being a component in a PMD compensator (first-order or all-order), 3) testing first-order compensators and DGD monitors, and 4) being a component in all-order PMD emulators. The simplest construction of a tunable DGD emulator comprises a polarization beam splitter (PBS) followed by a variable time-delay element in one branch and a polarization beam combiner (PBC), as illustrated in Fig. 1(a). Such bulk-optic-based configurations suffer disadvantages such as low speed, moving mechanical parts, and polarization instability, especially if an optical fiber is used in either of the two arms. Several new schemes for tunable DGD emulation have been proposed to overcome these problems [27]–[29]. A programmable DGD element based on birefringent crystals separated by magneto-optic (MO) switches, as shown in Fig. 1(b), has proven to be practical and useful in many PMD applications [27]. This approach will be described in detail in the next section.

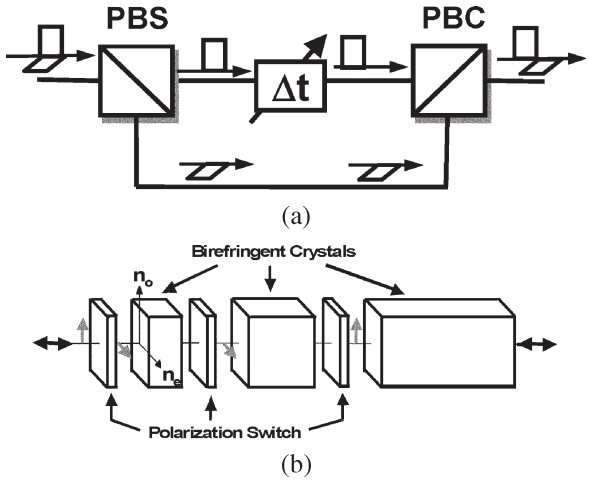

Fig. 1. (a) Tunable DGD emulator based on bulky optical components (PBS: polarization beam splitter; PBC: polarization beam combiner). (b) Conceptual diagram of a programmable DGD element using binary polarization switches and birefringent crystals.

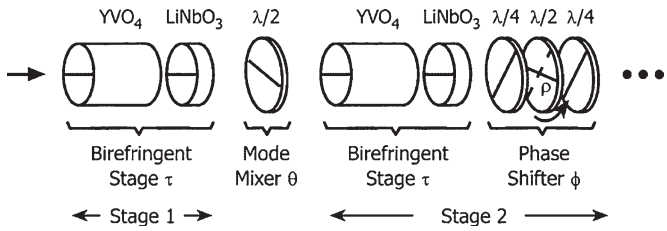

Fig. 2. First two stages of a four-stage coherent programmable PMD source (ECHO) (from [16]).

To construct a deterministic multiorder PMD emulator, Damask *et al.* employ a Fourier-based approach to the PMD generation [16]. They use a concatenation of four birefringent crystal sections separated by rotatable waveplates, as shown in Fig. 2, which they call "ECHO" for "enhanced coherent higher order" PMD instrument. The key component is the Evans phase shifter [33]: an element that is added after each crystal (excluding the two end sections) to bring the birefringent phase of each segment to within a small fraction of the beat length. Once the phase shifters are adjusted for coherence, they are rotated together to frequency shift the periodic DGD and/or higher order PMD spectra to deterministically generate the desired combinations of first-order and higher order PMDs. While the periodic behavior of this coherent PMD source could be a problem for the PMD emulation of WDM systems, this source provides a better coverage of the joint probability-density-function (pdf) space of DGD and SOPMD at a single wavelength when compared with other deterministic emulators.

Pure higher order PMD emulators are important for testing systems in which the first-order effects have been compensated. An interferometric configuration using tunable DGD elements, as shown in Fig. 3(a) [20], and a fiber-Bragg-grating (FBG)-based scheme, as shown in Fig. 3(b) [8], have been proposed for this purpose. The polarization controllers (PC1 to PC3) shown in Fig. 3(a) are used to align the PMD vectors in a triangle

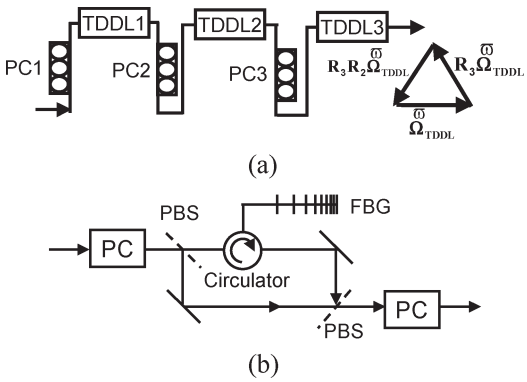

Fig. 3. (a) Interferometrically stable three-section higher-order PMD emulator (TDDL: tunable differential-delay line) (after [20]). (b) Isolated higher order PMD emulator using fiber Bragg gratings (after [8]).

between DGD sections (TDDL1 to TDDL3) to cancel all first-order effects at the center frequency. For the method illustrated in Fig. 3(b), pure first-, second-, or third-order PMD can be generated by incorporating a uniform FBG, a linearly chirped FBG, or a chirped FBG with a dispersion slope, respectively. In addition, an all-pass filter-based configuration was proposed that uses phase control and PBS/PBC elements [18] and is capable of generating first-order and higher order PMD effects as well as chromatic dispersion and dispersion slope.

Stability and repeatability are very difficult to achieve as the number of emulator sections becomes large. For this reason, emulators designed to deterministically generate DGD and higher order PMD components are typically made with fewer than four sections. As such, these emulators will not accurately mimic the statistics of the PMD in long single-mode fibers. Rather, they are used to repeatedly target a particular range of PMD values or combinations of first-order and higher order PMDs. It is also useful to expose a device under test to the full statistical variations that are expected to occur over long periods of time in optical fibers. All-order PMD emulators are required for this purpose.

C. All-Order PMD Emulators

Similar to theoretical models of optical fiber links using concatenated and randomly coupled piecewise linear birefringent sections, all-order PMD emulators may likewise be constructed by concatenating several linear birefringent elements (such as PMF sections, birefringent crystals, or even tunable DGD elements). To achieve different PMD states, some property of the emulator must be varied between samples such as the polarization coupling between sections, the wavelength, or the birefringent phase delay of each section. As the number of sections increases, the emulator statistics will converge toward those of a long single-mode fiber. Several configurations of all-order PMD emulators are illustrated in Fig. 4(a)–(f).

The configurations illustrated in Fig. 4 represent six models for constructing an all-order emulator.

1) *Fixed model:* Equal- or unequal-length sections of a phase-modulation (PM) fiber are spliced together at either random or 45° angles [33]. As explained in [9], the use of 45° angles leads to the most rapid frequency decorrelation of the resultant PMD vector, and the use of unequal sections avoids an undesired periodicity in the frequency ACF. This scheme has limited use, since different PMD states can only be obtained by widely varying the wavelength or by cycling through environmental changes.
2) *Rotator model:* Birefringent sections are randomly rotated relative to each other to obtain different PMD states. Examples include birefringent crystals mounted on rotation stages or separated by rotatable polarization mode mixers (thin waveplates) [13], PM fibers connected by rotatable connectors [14], and a long strand of the PM fiber with fiber twisters placed periodically along its length [12].
3) *Scattering model:* Birefringent sections are connected with polarization controllers that "scatter" the polarization state between sections according to a uniform distribution on the Poincaré sphere [17]. In addition to conventional emulators based on short birefringent sections and polarization scattering, a loop-synchronized polarization scattering has become a standard technique to replicate long-haul systems with correct polarization statistics using recirculating fiber loop testbeds [30], [31].
4) *Phase model:* The orientation between sections typically remains fixed at 45° (to obtain rapid frequency decorrelation), while the birefringent phase of each section is varied to obtain different PMD states. Examples of variable birefringent phase elements include voltage-controlled lithium-niobate crystals and PM fiber sections with small metallic heaters deposited on the fiber surface to temperature tune the birefringence [15].

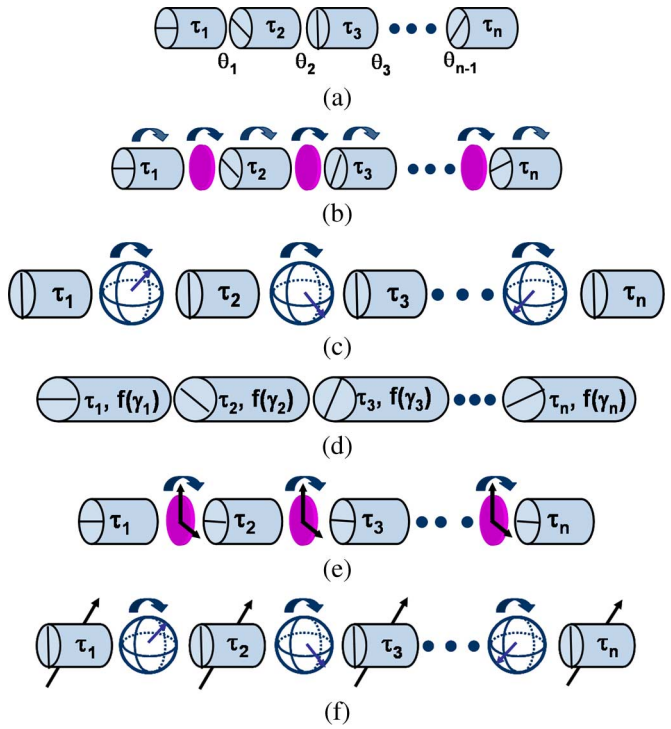

Fig. 4. Models of PMD emulators. (a) Fixed. (b) Rotator. (c) Scattering. (d) Phase. (e) Rotator + switch. (f) Tunable. (Color version available online at http://ieeexplore.ieee.org.)

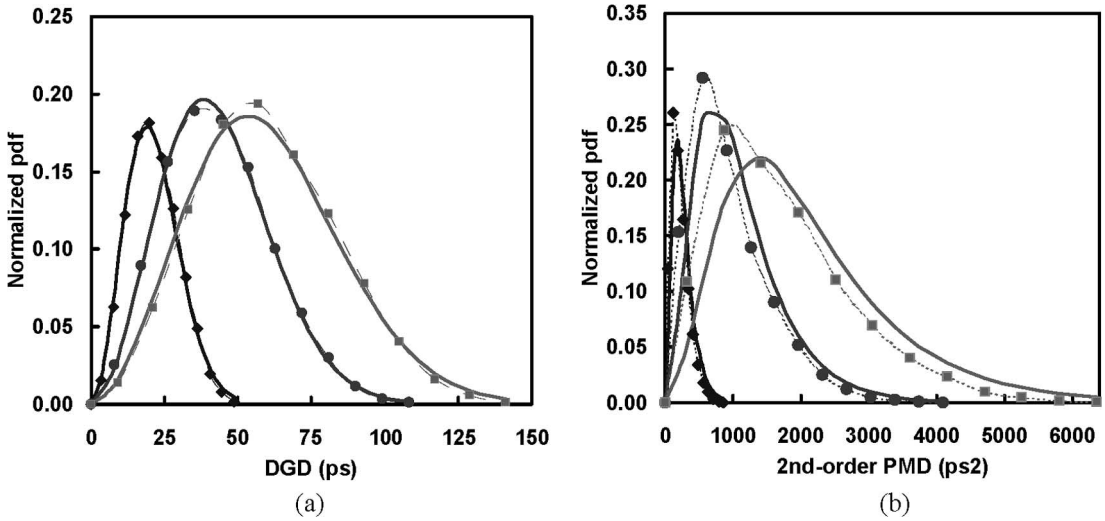

Fig. 5. Simulation results of a "rotator + switch" PMD emulator, as proposed in [26]. (a) DGD distributions with $\langle \Delta\tau \rangle = 21$, 43, and 60 ps. (b) Corresponding SOPMD distributions with $\langle \Delta\tau_\omega \rangle = 215$, 937, and 1705 ps^2, respectively. All of the distributions were obtained from the same emulator.

The coherent PMD source described in the section on isolated-order emulators is also a hybrid of the phase and rotator all-order emulator models.

5) *Rotator + switch model:* This configuration is similar to the rotator model, in which fixed DGD sections are connected by continuous variable polarization rotators (0° to 180°), to provide PMD emulation with a designed average PMD. In this case, however, the rotators can also operate as binary switches to cancel or add the DGD of neighboring sections. This enables an alternative type of rotation-based emulator in which the emulator can be reconfigured to obtain different average PMD values. With different combinations of rotators and switches between sections, different statistical distributions may be obtained using a single setup [26]. The cost of this added flexibility is the need for many more birefringent elements, since at least 10 to 15 equivalent DGD sections (either individual or through canceling/adding neighboring sections) are needed to produce accurate PMD statistics. Further, the number of equivalent sections may be different for different statistics, and the overall performance (deviation from ideal distributions, autocorrelation, etc.) may also change. The optimal design of this type of emulator is still under investigation. Fig. 5 shows an example of three different distributions of DGD and SOPMD generated by this type of emulator, as described in [26].
6) *Tunable model:* The average DGD values of the emulator modes in Fig. 4(a)–(d) are fixed at the time of fabrication and cannot be reconfigured to emulate different fiber plants. A tunable model using tunable DGD supersections to replace the fixed ones was proposed in [17] and [24]. The proposed model uses polarization controllers inserted between tunable-DGD sections to "scatter" the polarization state according to a uniform distribution on the Poincaré sphere. By tuning the DGD values of each section according to a Maxwellian distribution and randomly varying the polarization controllers between data samples, the emulator will generate an exact Maxwellian DGD distribution (and corresponding SOPMD distributions if enough supersections are used). Tunable statistics (different average PMD values) can therefore be obtained by applying proper DGD distributions to each tunable-DGD section. Such reconfigurability allows one to emulate the PMD of different fiber plants with a single emulator.

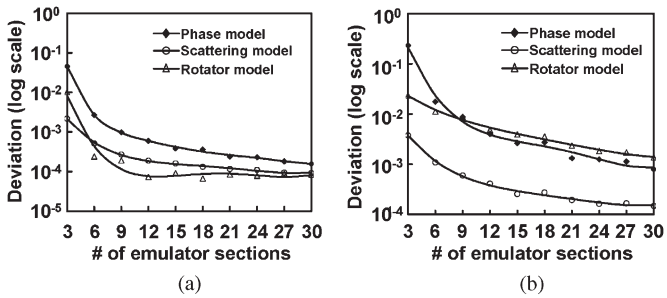

Fig. 6. Comparison of three emulator models: the rotator, scattering, and phase models [15]. The plot shows the deviation from the statistical distributions expected from a real fiber with the same average DGD versus the number of emulator sections. (a) DGD deviation from Maxwellian. (b) SOPMD magnitude deviation from theory.

A major limitation of all-order PMD emulators is that the finite number of sections puts a cap on the maximum DGD that can be obtained by the emulator. This peak value corresponds to the case when the birefringent axes of all the emulator sections become aligned. The peak DGD value is approximately the product of the rms DGD of the emulator sections and the square root of the number of sections. A single-mode fiber contains hundreds to thousands of birefringent sections [34]; therefore, emulators will always tend to have a maximum DGD that is much less than in an actual fiber, causing a deviation from real fiber statistics [15], [35]. For example, Fig. 6 shows a comparison of the "rotating," "scattering," and "phase" (using microheaters) models in terms of the absolute deviation from the statistical distributions expected from a real fiber.

Another limitation of statistical all-order emulators is that an impractical number of random samples must be taken to

encounter several rare PMD events. Even with Monte Carlo computer simulations, it is prohibitively time consuming to perform enough trials to fully evaluate the effects of PMD events that cause outage probabilities of 10^{-6} ($<$ 1 min/yr) or less. To efficiently emulate these rare events, various methods have been proposed including importance sampling (IS) and multicanonical (MCC) sampling [36], [37]. For example, with IS, extremely rare events with probabilities as low as 10^{-20} are easily obtained with experiments or computer simulations [36].

III. Programmable DGD Elements for Emulators With Tunable PMD Statistics

As mentioned previously, tunable DGD elements are essential for various applications in the PMD emulation. For practical applications, the desired properties include repeatability, fast control speed, and good optical characteristics such as low insertion loss, low polarization-dependent loss (PDL), and wavelength-dependent loss. The programmable DGD element described in [27] has demonstrated such figures of merit. As shown in Fig. 1(b), the element consists of multiple birefringent crystal sections ("delay sections") separated by MO switches. The arrangement of the crystal lengths follows a binary power series with a factor of two (either increasing or decreasing), enabling digital programmability of the total delay value. The MO switches rotate the polarization state between crystals by 0° or 90° with the application of one of two different saturation currents. Thus, at the input to each section, the SOP can be switched to align with the slow or fast axis of the subsequent birefringent crystal, thereby adding to or subtracting from the total DGD of the device, without adding higher order PMD.

The programmable DGD module we demonstrated in [27] uses six birefringent crystals (i.e., a six-bit module) and can generate tunable DGD values from -45 to $+45$ ps with a resolution of 1.40 ps (a six-bit version with a range of 0–22 ps and a resolution of 0.34 ps has also been constructed). The module has a fast response time on the order of 1 ms. The static optical characteristics are good, with $<$ 1.2-dB insertion loss, $\sim$0.2-dB PDL, and $<$ 0.15-dB wavelength-dependent loss across the c-band. As shown in Fig. 7(a), due to the binary nature of the module, the generated DGD values agree well with the designed DGD values, and each DGD value is exactly reproducible (highly repeatable). Also, the SOPMD is negligibly small (typically < 85 ps^2).

Excellent dynamic performance can also be obtained by using a parallel bit-by-bit switching and by optimizing the arrangement of the crystals (decreasing or increasing lengths from input to output). The module was evaluated in a 10-Gb/s NRZ system under static conditions and under a worst case scenario of rapidly switching between neighboring DGD states. The resulting power penalties measured using an optical preamplified receiver for both cases are shown in Fig. 7(b). An additional power penalty of less than 0.2 dB results in the worst case scenario due to transient effects during the switching. Note that this result can only be achieved when the light is input from the crystal with the longest length (i.e., decreasing lengths along the transmission).

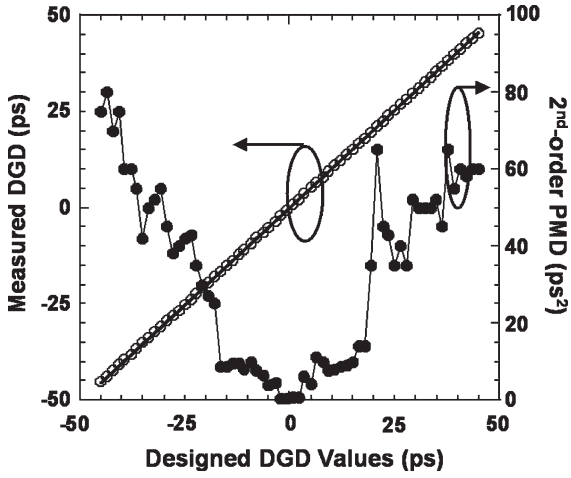

(a)

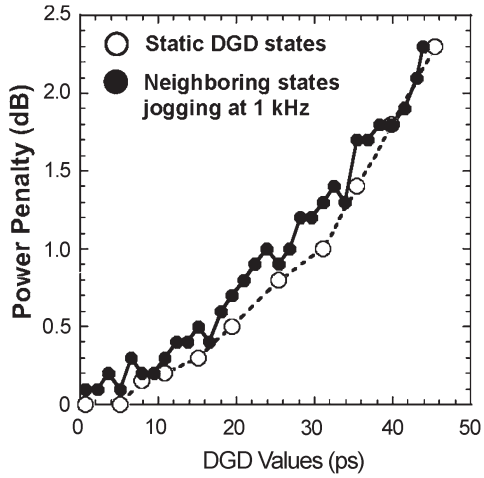

(b)

Fig. 7. Typical characteristics of the programmable DGD element. (a) Measured DGD and SOPMD as a function of the designed DGD values. (b) Dynamic performance in a 10-Gb/s NRZ system: Power penalties measured using an optical preamplified receiver of static DGD states (open circles) and dynamic switching ("jogging") between neighboring states at 1 kHz (solid circles).

Based on the tunable model, we use three of these programmable DGD elements separated by two fiber-squeezer-based polarization controllers to construct an all-order PMD emulator with tunable statistics [17]. Fiber-squeezer-based polarization controllers can generate a uniform polarization scattering between sections [38], and have intrinsic advantages such as low (activation) loss, low PDL, and fast response time. Applying a Maxwellian distribution with an average $\Delta\tau$ to each element yields an average DGD of $3^{1/2}(\Delta\tau)$ for the total emulator and a corresponding SOPMD distribution that falls slightly short of that expected for a real fiber [39]. Three different (i.e., tunable) statistical distributions are shown in Fig. 8(a) (DGD) and Fig. 8(b) (SOPMD) with $\langle \mathrm{DGD} \rangle = 10$, 25, and 35 ps. The corresponding SOPMD distributions have averages of 38, 268, and 471 ps^2, respectively, which are $\sim$30% lower than expected for real fibers with the same average DGD values. Simulation results in Fig. 8(c) show the deviation from the ideal SOPMD distribution and background autocorrelation as the number of tunable DGD sections is increased [24]. When

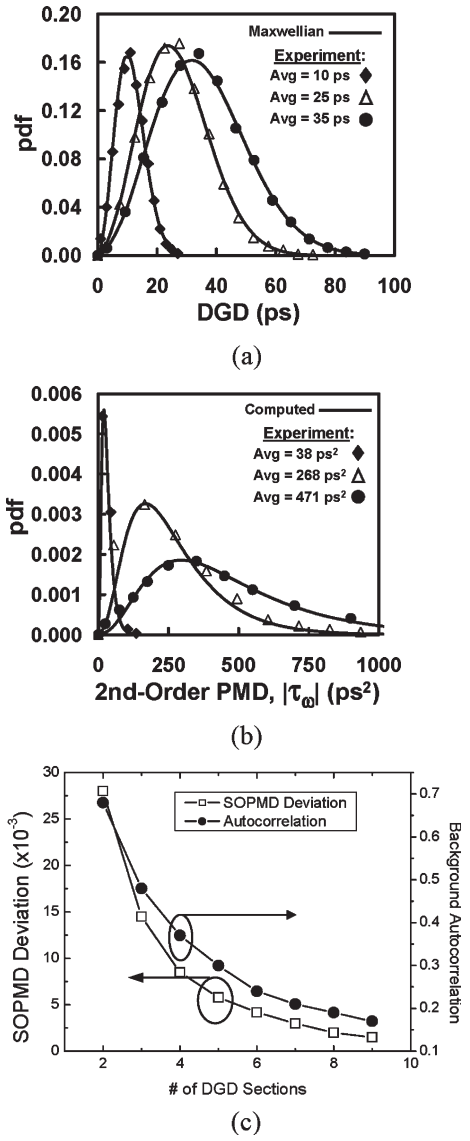

Fig. 8. Tunable statistics generation with a PMD emulator constructed from three programmable DGD elements and polarization controllers. (a) Experimental results for three different DGD statistics with $\langle \Delta\tau \rangle = 10, 25,$ and 35 ps. (b) Corresponding SOPMD distributions with $\langle \Delta\tau_\omega \rangle = 38,\ 268,$ and 471 ps^2, respectively. (c) Simulation results of the SOPMD deviation from the ideal SOPMD pdf and background autocorrelation as a function of the number of tunable DGD sections (after [24]).

the number of sections exceeds six, the deviation is < 0.005, and the correlation of the PMD vectors for different WDM channels (channel spacing > 0.4 nm) is less than 20%.

The PMD state of this tunable-statistics emulator remains stable and repeatable over a period of several hours. However, the mapping between the emulator control parameters and the output PMD does not remain intact with large temperature changes, or if the single-mode fiber pigtails between sections are perturbed. Though the DGD of each tunable element is well known, the birefringent phase between sections is not controlled to within a beat length, making it impossible to deterministically control the angles between the PMD vectors of each section. To create a truly repeatable emulator in which any previously recorded set of PMD values can be dialed-in at later point in time, we insert simple in-line polarimeters between sections (Fig. 9) [40]. Since the DGD of each section is known and is extremely stable (< 0.1 ps$/80\ ^\circ$C), the additional SOP information allows us to construct a lookup table of output first and SOPMD vectors versus the six input DGD and SOP parameters. An automated system can then be used to adjust the DGD elements and polarization controllers, while monitoring the polarimeters, to dial-in a desired PMD state. The effectiveness of this approach has been demonstrated in [25], though the tracking accuracy and the size of the lookup table remain challenging issues.

IV. Advanced PMD Emulation

During recent years, various advanced emulation techniques have been proposed to more efficiently obtain rare PMD events, both experimentally and with numerical simulations. These techniques include the importance sampling (IS) [36], [41], [42], multicanonical (MCC) sampling [37], [43], [44], the Brownian-bridge (BB) method [45], and the very recent hinge model [46]–[48].

The IS is a powerful tool for obtaining very low probability events with relatively few sample points [36]. This is accomplished by biasing the method of obtaining random samples, such that the statistical results are concentrated in the area of interest in the sample space. For PMD emulation, the IS method is used to bias the coupling angle between the PMD vectors of adjacent sections in order to preferentially align them to obtain rare PMD events. The process is illustrated in Fig. 10(a). The IS for the first-order PMD is achieved by biasing the angle θ_n to preferentially align $\mathbf{\Omega}_n$ and $\mathbf{\Delta\Omega}_{n+1}$. The IS for SOPMD is accomplished by biasing $\mathbf{\Delta\Omega}_{n+1}$ to be parallel to μ_3, the condition for maximum SOPMD [see Fig. 10(a) for the detailed coordinate system]. IS models typically implement the emulators with a constant DGD per section. If the emulator sections are instead constructed from variable DGD elements, then the DGD per section can be further biased toward large values to obtain even higher efficiency. This concept was first demonstrated experimentally using a tunable-statistics PMD emulator [17], with a corresponding simulation model built later by Biondini and Kath [42]. The experimental approach of this model will be discussed later in detail.

The MCC sampling is an iterative technique that progressively samples the small probability region of a system variable, such as the DGD, by approaching a random walk in the values of the input control variables [37]. Each new system realization is obtained from the preceding realization through a Markov process, in which the acceptance rule is determined by the pdf estimate obtained at the prior iteration step. At the end of the calculation, all regions of the control variable space are visited with equal probability. The conceptual diagram of the MCC procedure is shown in Fig. 10(b). An initial distribution $p^{(0)}$ is first assumed for the pdf of the measured system variables. Arbitrary initial values are then chosen for these variables, which are collectively denoted as the state i. Applying a random perturbation to these variables yields a new state k; this transition is accepted with a probability given by the minimum of one and the ratio of the current estimates of the pdf for the states i and k. If the transition is rejected, the old state

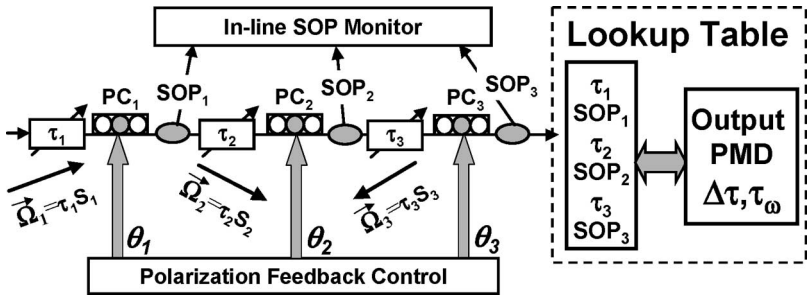

Fig. 9. Emulator setup incorporating simple in-line polarimeters with automatic feedback to control the SOP between sections to enable the generation of a lookup table of input DGD and SOP values versus output DGD ($\Delta\tau$) and SOPMD (τ_ω) values.

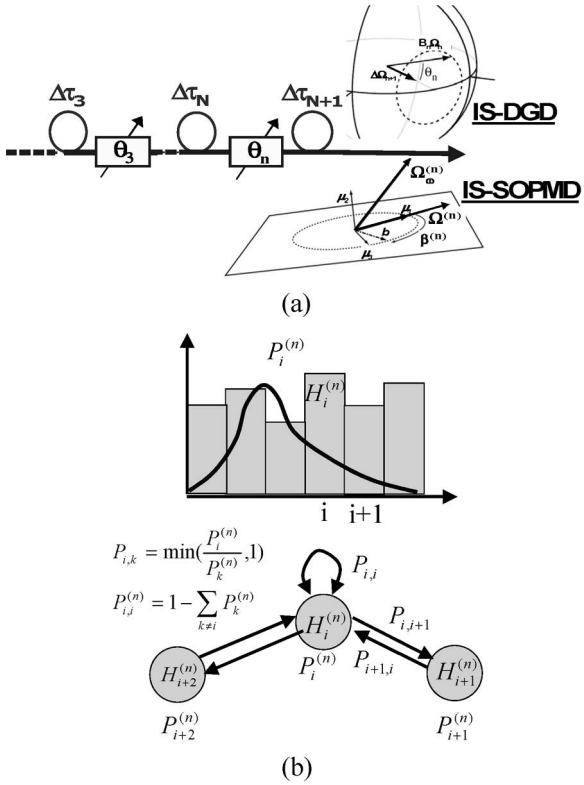

Fig. 10. (a) IS method using preferential alignment of PMD vectors. (b) MCC procedure.

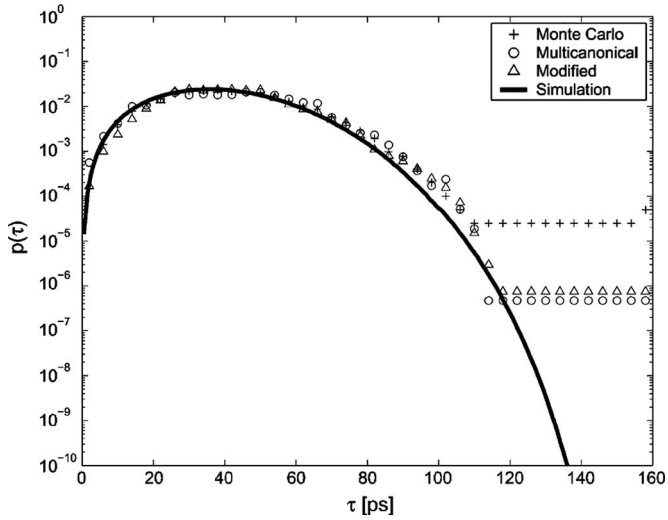

Fig. 11. Experimental comparison of MCC sampling techniques with a conventional Monte Carlo method using a 30-section PMD emulator (from [43]).

is instead employed in the subsequent step. After a specified number of steps, a histogram $H^{(n)}$ of the number of times that states in each interval of the system variables (DGD) are visited is constructed, and the pdf for the next iteration is obtained from $p^{(n+1)} = C^{(n)} p^{(n)} H^{(n)}$, where $C^{(n)}$ is an appropriate normalization factor.

Theorists have performed extensive studies of these advanced emulation tools from different perspectives through computer simulations, while system designers are more interested in practical experimental approaches for network evaluation and optimization. The efficiency of IS is extremely high, but the lack of programmability, stability, and repeatability of most emulators makes the realization of experimental IS impossible. Specifically, deterministic control of the coupling angle between the PMD vectors of adjacent sections is needed. The efficiency of the MCC method is generally lower than IS, but the MCC does not require a deterministic control, it only requires that the properties of the emulator do not vary substantially over time. Further, the MCC procedure does not require previous knowledge of the form of the pdf. Due to these relatively relaxed requirements, this procedure was demonstrated using a 30-section PMF-based statistical emulator, for which the repeatability and long-term stability are not the key properties [43]. The resulting DGD distribution is shown in Fig. 11 and reached a probability of 10^{-6} with only 8000 samples.

As discussed, it would be extremely difficult to deterministically control the polarization coupling between sections using most PMD emulators (i.e., those with fixed DGD sections) to perform experimental investigations using the IS technique. Thus, we proposed a new approach based on our tunable PMD emulator (T-PMDE) to readily enable the experimental IS to produce low-probability events without the need to determine and control the direction of the PMD vector between sections. This is accomplished by simply biasing the distribution of the DGD values applied to each element and uniformly scattering the polarization coupling between sections.

This experimental IS technique is conceptually illustrated in Fig. 12 using a T-PMDE with three programmable DGD elements connected by polarization controllers. The programmability of the DGD elements is exploited to perform the IS by applying randomly selected DGD values from a pdf other

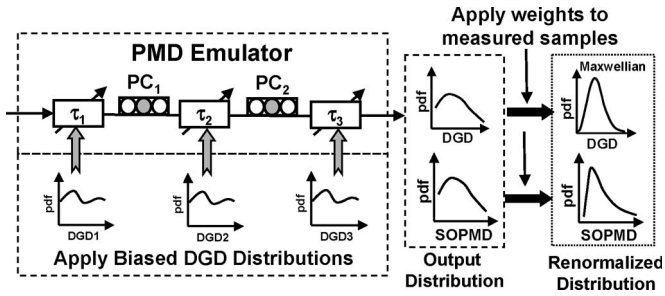

Fig. 12. Conceptual diagram of applying the IS method to the T-PMDE, which is accomplished by applying a biased DGD distribution to each section and then appropriately weighting the results to obtain the desired pdf.

than a Maxwellian. The applied pdf is chosen to generate more output samples in the region of interest with the fewest possible measurements. The DGD applied to each element and the corresponding output DGD and SOPMD are recorded for each sample. As expected, the measured output values will not follow the desired Maxwellian distribution. As a postprocessing step, the measured samples are properly weighted to adjust their probabilities to match the desired Maxwellian statistics. For each DGD section, let $p(x_i)$ be the probability of obtaining DGD x_i using the desired Maxwellian pdf (with an average DGD of $\Delta\tau = \langle \mathrm{DGD} \rangle / (3^{1/2})$). Let $p^*(x_i)$ be the probability using a uniform pdf. For each sample i, three likelihood ratios are computed, $p(x_i)/p^*(x_i)$, where x_i corresponds to the DGD values applied to the three sections. The three ratios are multiplied together and divided by the total number of samples to determine the weight for each sample. The output DGD values are then sorted while keeping track of the corresponding weights. The DGDs and corresponding weights are grouped into DGD bins, and the weights in each bin are summed to obtain the probability for that bin. These probabilities are then plotted alongside a Maxwellian, integrated over each bin, for comparison. Similar data processing procedures are applied for the SOPMD.

To efficiently obtain PMD events covering the entire range from low-to-high values, we employed the technique of "multiple importance sampling" to combine the results of several IS experiments, each using a different DGD pdf applied to the sections: An unbiased Maxwellian pdf was used to obtain several values in the low-DGD region, a negatively sloped linear pdf was used to obtain low-to-medium DGDs, and a positively sloped pdf was used to obtain high DGDs. 840 samples were taken for each distribution. The experimental results are weighted to obtain the distributions of DGD and SOPMD shown in Fig. 13(a) and (b). The multiple IS technique provides a better coverage of the entire sample space. The resulting distribution tail extends to 10^{-30} with only $\sim$2500 measurement samples.

A similar concept is used to characterize the impact of the PMD on the statistics of the system Q for both average and extremely rare PMD events [17].

PMD models presented so far are well known and accepted for PMD investigations. Several recent publications and talks highlight another system model that may more accurately represent real systems most of the time [46]–[48]. This model, as depicted in Fig. 14(a), assumes that the PMD along a single buried fiber route ($<$ 100 km) only varies significantly over a period of weeks, or even months, essentially remaining frozen over these timescales. Any significant variations in the PMD are assumed to occur in cascaded multiple fiber spans with finite numbers of rotation points, or "hinges" (such as amplifier huts or bridges). Under this scenario, simulations show that for ten statistically independent channels in a six-segment system, most of the channels will have a zero probability of exceeding 2.5 times τ_{rms} [Fig. 14(b)] [47]. Such non-Maxwellian behavior is pushing researchers to emulate and investigate PMD effects using this new model.

Most available PMD emulators are not suitable for emulating PMD under the hinge model because of poor stability and the difficulty of obtaining slow or small PMD variations after cascading several emulator sections. Even for the T-PMDE, due to its random nature (random DGD generation in each section and random polarization coupling between sections), the generated PMD often changes dramatically from sample to sample.

To simulate the "Hinge" model using the T-PMDE, a typical configuration is depicted in Fig. 15(a). Each PMDE section provides slow dynamics (both PMD and polarization evolution) and a few dynamic polarization controllers that generate dramatic polarization variations to act as the "hinges" ("Hinge"-PC). The challenge remains for a tunable emulator itself to emulate slow environmental perturbations (i.e., slow dynamics). To accomplish this, the control algorithm is redesigned for both the DGD and fiber-squeezer-based polarization controller sections of the emulator. Specifically, the DGD values applied to each section are reorganized (but still follow a Maxwellian distribution, in general), and slow polarization coupling is implemented [49]. A group of DGD values that have a Maxwellian distribution is first generated for a predefined total number of samples. These samples are divided into several subgroups, depending on the total sample number. Each subgroup is sorted following a slow-variation pattern from sample to sample [Fig. 15(b)]. The evolution of each DGD element is different in order to preserve the random nature of the PMD and to minimize distortion of the total statistics. Slow polarization coupling is easily achieved using a conventional sinusoidal driving of each fiber squeezer section, with different peak-to-peak voltages and frequencies for each. Thus, polarization coverage of the whole Poincaré sphere is not sacrificed.

Using the above approach, the generated first-order PMD still follows a Maxwellian distribution with a negligible distortion, with an average value of 29 ps (close to the designed value of 30 ps), while the dynamics of the PMD statistics are dramatically slowed down. Fig. 16(a) shows the DGD variation from sample to sample for the dynamic model, and Fig. 16(b) shows the variations for the slow model. Similar slow dynamics are found for the SOPMD [49], indicating that this method can be successfully applied to the experimental configuration shown in Fig. 16(a) to emulate the PMD under the "hinge" model for system investigations.

In addition to using this T-PMDE with programmable DGD elements to experimentally implement the IS and hinge models, it can also be adapted for the PMD emulation with

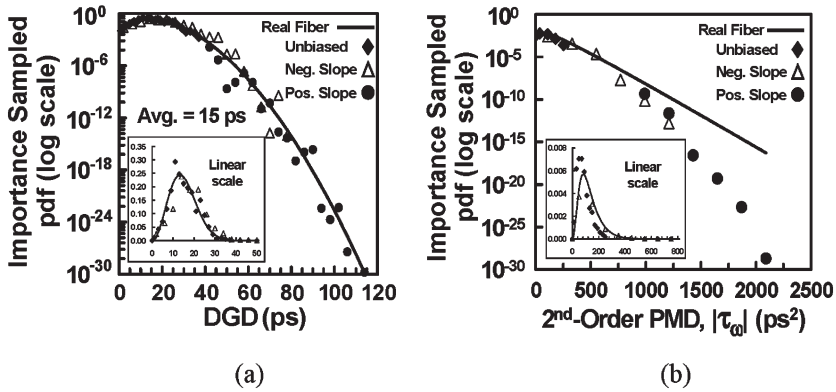

Fig. 13. Experimental results using multiple IS to provide a better coverage through the entire sample space. Three DGD distributions applied to each section (840 samples/each). (a) Resulting DGD distribution showing that each pdf generates samples in different regions to cover the entire Maxwellian, and (b) resulting SOPMD pdf. The insets show the pdfs on a linear scale.

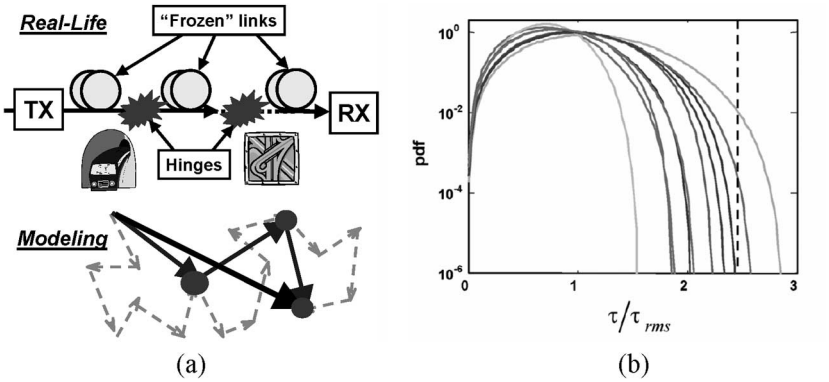

Fig. 14. (a) "Hinge" model in which most of the spans remain frozen over weeks, or months, and several dynamic "hinges" exist that are responsible for any significant changes in the PMD. (b) Sample DGD pdfs for ten statistically independent channels in a six-segment system indicating that most of the channels have a zero probability of exceeding 2.5 $\tau_{\rm rms}$ (from [47]).

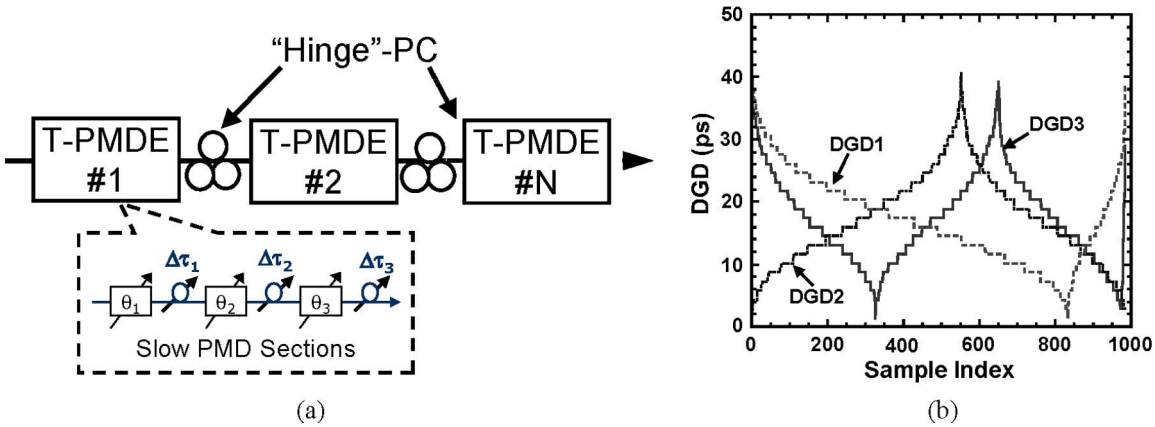

Fig. 15. (a) Conceptual diagram of a "hinge" emulator using multiple T-PMDE containing programmable DGD elements (T-PMDE) with slow PMD dynamics. (b) To realize the slow PMD dynamics for a single tunable emulator [T-PMDE shown in 16(a)], the DGD evolution is reorganized for three DGD elements with slow variations from sample to sample (∼1000 samples). (Color version available online at http://ieeexplore.ieee.org.)

the MCC technique and the BB model. It would also be of interest to use this flexible emulator to compare various PMD mitigation and compensation schemes using these advanced models (IS, MCC, and BB), since the events that occur in the tails of the PMD probability distributions after compensation are of significant interest to the community.

V. Tunability in PMD Compensation

Tunable DGD is not only an attractive feature for the PMD emulation but is also desirable for the compensation of PMD effects in optical fiber systems. A typical first-order PMD compensator consists of a polarization controller followed by either a fixed or a variable DGD element. A variable compensator

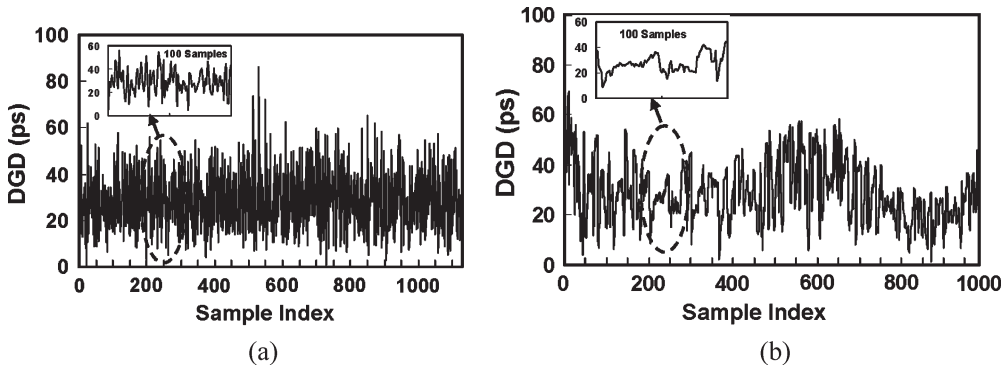

Fig. 16. Comparison of generated PMD dynamics (negligible distortion on the overall PMD distribution). (a) Previous approach using random DGD and random polarization coupling as described in Section III. (b) Slow PMD dynamics approach.

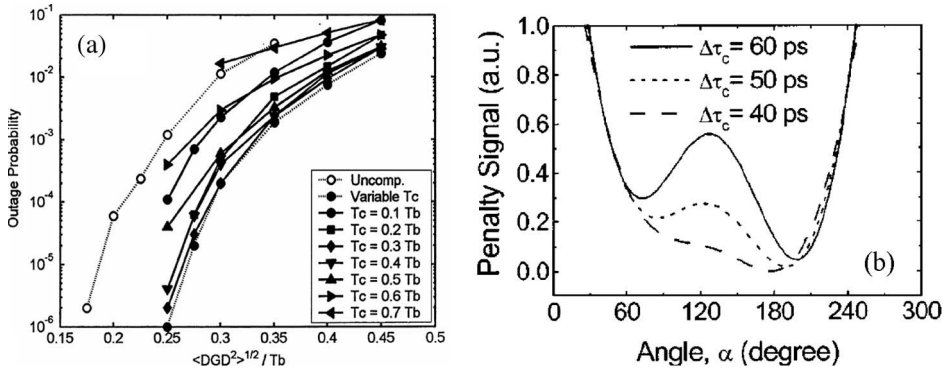

Fig. 17. Benefits to first-order PMD compensation using tunable DGD elements. (a) Comparison of outage probability with fixed and tunable DGDs in 33% duty cycle OOK-RZ transmission systems (Tc: delay line length; Tb: bit period) (from [50]). (b) Diagram illustrating the existence of local minimums during tracking using fixed DGD compensator (α is the angle between the fiber and compensator PMD vectors) (from [51]).

can always optimize the system performance under different average PMD values, while a fixed one offers a limited improvement. For example, Fig. 17(a) shows a comparison of the performance of PMD compensators with different fixed DGD values with one that incorporates a variable DGD element [50]. Though an optimum compensation value exists for various link conditions, the additional degree of freedom, provided by a variable DGD element, increases the compensation possibilities. For example, variable DGD-based PMD compensators can reduce the risk of feedback loops being trapped in a locally optimized state, as shown in Fig. 17(b) [51].

In cases where polarization scrambling at the transmitter is used to facilitate the PMD compensation by reducing the complexity and increasing the stability of the feedback control, a variable DGD element is always required in order to exactly cancel out the fiber's DGD [52], [53]. Furthermore, as higher order PMD effects become more significant, variable DGD elements may be required for higher order PMD compensation as well [54]–[56]. Several previous publications have compared various compensation schemes including both first-order and higher order compensations [54]–[57].

Tunable DGD elements have been used in several experimental demonstrations for both first-order and higher order compensations [52], [58]. Notably, a programmable DGD equalizer that is similar in construction to our DGD element was used in a recent demonstration of a PMD compensation scheme in a 160-Gb/s OTDM transmission system using the RZ-DPSK format [52]. A schematic illustration of the equalizer is shown in Fig. 18. Only four birefringent crystals (four-bit) and three MO rotators are needed. As in our DGD module, the crystals are placed with their lengths in decreasing order for improved dynamic performance. Negligible distortion is observed during switching when a decreasing-length series is used, whereas the PMD vectors are distorted during switching for the increasing length arrangement.

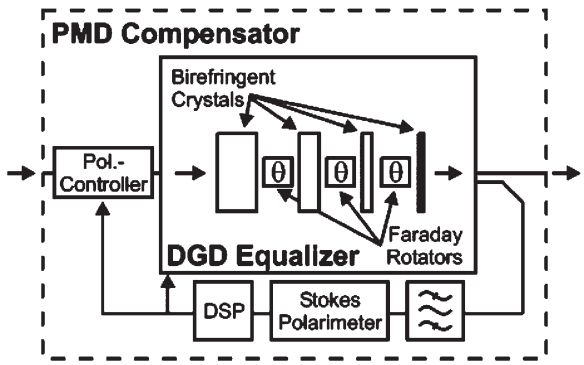

Fig. 18. First-order PMD compensator based on birefringent crystals, MO polarization rotators, a $LiNbO_3$ polarization controller, a bandpass filter, a polarimeter, and a digital signal processor (DSP) (from [52]).

Though many PMD compensation schemes in the optical domain have been proposed, simulated, and demonstrated to show improvements in PMD tolerance, the real bottleneck for PMD

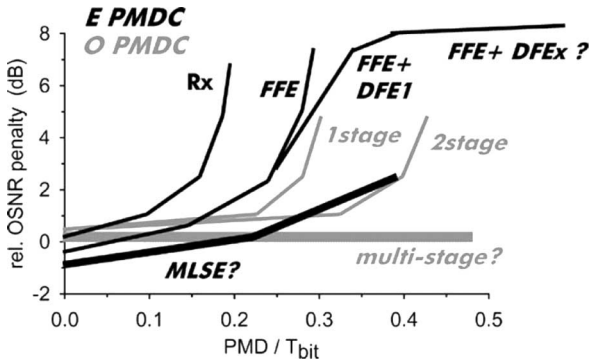

Fig. 19. Estimated penalty versus PMD-limits of electronic (dark lines, E-PMDC) and optic (shaded lines, O-PMDC) PMD compensators (from [67]). (FFE: feed-forward equalizer; DFE: decision feedback equalizer; and MLSE: maximum likelihood sequence estimation).

compensation is the control algorithm. The key requirements for a practical algorithm (with feedback [52], feedforward [59], or both [53]) include a fast response time (millisecond scale), reset-free control (no loss of signal), and global optimization. As the number of degrees of freedom in a PMD compensator increases, the theoretically achievable performance improves, but the control algorithm becomes prohibitively complicated [60], [61]. In addition, the control algorithm is highly correlated with or dependent upon the monitoring signal. Xie and Moller compared the performance of a one-stage PMD compensator with different feedback signals in various modulation systems [61]. They found that most conventional monitoring methods (DOP with filtering, RF, and eye opening) can achieve very close performance after an optimized feedback control. Effective PMD monitoring techniques that can isolate different degrading effects and help reduce the complexity of practical control algorithms are also important areas of research for PMD compensation [62].

VI. Discussion and Conclusion

As the data rate per optical channel increases, solving the PMD-induced degrading effects will become more and more challenging. In addition to the PMD emulation and compensation strategies discussed above, several related technologies are needed to evaluate and combat the effects of PMD. These include efficient and endless polarization control, effective and fast PMD monitoring, and mitigation of combined effects [62]–[64]. While a significant progress has been made in both research laboratories and deployed systems during the last decade, several issues remain uncertain at this point.

1) *Optics or electronics:* Both the PMD monitoring and compensation can be done either by electronics or optics [65]–[67]. Electronic solutions have intrinsic advantages such as low cost and stable performance while they suffer from bit-rate dependence and limited improvement. Optical solutions are typically independent of data speed and can maximize the optimization limits, but struggling to lower costs and to design practical algorithms are major concerns. Fig. 19 shows an estimated performance comparison of various electronic mitigation methods and optical approaches [67]. Recent simulation and measurement results indicate that some differences (e.g., MLSE and FFE/DFE) are not that pronounced.

   Currently, cost-effective electronic mitigation schemes at 10 Gb/s are promising, while at higher data rates, the complexity and cost of electronics make the optical solutions better candidates. Therefore, tradeoffs between cost and performance must be made for deploying PMD solutions.
2) *Single channel or multichannel:* In general, the polarization states of different channels in a multichannel system are uncorrelated and randomly distributed. Thus, when only one PMD compensator is used, it would seem impossible to optimize all channels simultaneously to the same performance as in a single-channel system, or even to optimize one of the channels without degrading others. While, so far, several approaches for multiple-channel PMD compensation have been proposed and demonstrated [68]–[71], the feasibility in practical systems is still unknown. Since a single PMD compensator for a WDM system cannot have the same performance as for a single channel, again, the cost of PMD compensators is a barrier to be considered, as well as whether or not the multichannel PMD compensation is necessary.
3) *Maxwellian or non-Maxwellian:* Most PMD models are built on the assumption of a Maxwellian DGD distribution. However, as the "hinge" model illustrates, systems can become non-Maxwellian, in which case, related PMD studies will need to be reevaluated as with our understanding of outage probabilities [48]. Both models have been legitimized with real measurements, but the following question remains: Which one represents most embedded systems more accurately so that it can be used as a guide for system design, evaluation, and optimization?
4) *PMD and other effects:* The PMD itself is a major hurdle for high-performance systems, but there are many other degrading effects, some of which may interact with PMD, and make the situation even worse. For example, PDL and fiber nonlinearities are two such phenomena that receive much attention in the literature [72]–[75]. These additional effects may invalidate solutions for pure PMD; therefore, we need to consider in system studies and applications.

In summary, programmable DGD elements are versatile tools for optically emulating and compensating PMD effects. They have been successfully incorporated in various applications, many of which were made possible because of the tunability of the DGD elements. We reviewed several different models of PMD emulators and focused on using programmable DGD elements to enable the advanced emulation techniques that are of great interest for evaluating systems with or without the PMD compensation (electronic or optical). Tunable DGD assisted PMD compensation configurations (either first order or higher order) showed improved performance over those using fixed DGD elements, while compensation algorithms facilitated by the PMD monitoring methods remain a major practical issue for optical PMD compensators.

ACKNOWLEDGMENT

The authors would like to thank Prof. W. L. Kath (Northwestern University), Prof. D. Yevick (University of Waterloo), and Dr. Y. Shi (Boeing Satellite Systems).

REFERENCES

[1] S. Ferber, C. Schubert, R. Ludwig, C. Boemer, C. Schmidt-Langhorst, and H. G. Weber, "640 Gb/s DQPSK single-channel transmission over 480 km fiber link," in *Proc. ECOC*, 2005, vol. 3, pp. 437–438.

[2] H. Kogelnik, R. M. Jopson, and L. E. Nelson, "Polarization mode dispersion," in *Optical Fiber Telecommunications IVB*, I. P. Kaminow and T. Li, Eds. San Diego, CA: Academic, 2002, ch. 15.

[3] C. D. Poole and J. Nagel, *Optical Fiber Telecommunications*, vol. III-A. San Diego, CA: Academic, 1997, ch. 6, pp. 114–161.

[4] G. J. Foschini and C. D. Poole, "Statistical theory of polarization dispersion in single mode fibers," *J. Lightw. Technol.*, vol. 9, no. 11, pp. 1439–1456, Nov. 1991.

[5] H. Bülow, W. Baumert, H. Schmuck, F. Mohr, T. Schulz, F. Küppers, and W. Weiershausen, "Measurement of the maximum speed of PMD fluctuation in installed field fiber," in *Proc. OFC*, San Diego, CA, Feb. 1999, pp. 83–85.

[6] M. Boroditsky, M. Brodsky, N. J. Frigo, P. Magill, and H. Rosenfeldt, "Polarization dynamics in installed fiberoptic systems," in *Proc. IEEE LEOS*, Sydney, Australia, 2005, pp. 414–415.

[7] D. A. Nolan, X. Chen, and M. J. Li, "Fibers with low polarization-mode dispersion," *J. Lightw. Technol.*, vol. 22, no. 4, pp. 1066–1077, Apr. 2004.

[8] H. Kogelnik, L. E. Nelson, and J. P. Gordon, "Emulation and inversion of polarization-mode-dispersion," *J. Lightw. Technol.*, vol. 21, no. 2, pp. 482–495, Feb. 2003.

[9] I. T. Lima, R. Khosravani, P. Ebrahimi, E. Ibragimov, C. R. Menyuk, and A. E. Willner, "Comparison of polarization mode dispersion emulators," *J. Lightw. Technol.*, vol. 19, no. 12, pp. 1872–1881, Dec. 2001.

[10] A. E. Willner and M. C. Hauer, "PMD emulation," in *J. Opt. Fiber Commun. Rep.*, vol. 1, C. R. Menyuk and A. Galtarossa, Eds, Nov. 2004, pp. 181–200.

[11] M. Karlsson and J. Brentel, "Autocorrelation function of the polarization-mode dispersion vector," *Opt. Lett.*, vol. 24, no. 14, pp. 939–941, Jul. 1999.

[12] R. Noé *et al.*, "Polarization mode dispersion compensation at 10, 20, and 40 Gb/s with various optical equalizers," *J. Lightw. Technol.*, vol. 17, no. 9, pp. 1602–1616, Sep. 1999.

[13] J. N. Damask, "A programmable polarization-mode dispersion emulator for systematic testing of 10 Gb/s PMD compensators," in *Proc. OFC*, Baltimore, MD, Mar. 2000, pp. 28–30.

[14] R. Khosravani, I. T. Lima, Jr., P. Ebrahimi, E. Ibragimov, A. E. Willner, and C. R. Menyuk, "Time and frequency domain characteristics of polarization-mode dispersion emulators," *IEEE Photon. Technol. Lett.*, vol. 13, no. 2, pp. 127–129, Feb. 2001.

[15] M. C. Hauer, Q. Yu, E. R. Lyons, C. H. Lin, A. A. Au, H. P. Lee, and A. E. Willner, "Electrically controllable all-fiber PMD emulator using a compact array of thin-film microheaters," *J. Lightw. Technol.*, vol. 22, no. 4, pp. 1059–1065, Apr. 2004.

[16] J. N. Damask, P. R. Myers, A. Boschi, and G. J. Simer, "Demonstration of a coherent PMD source," *IEEE Photon. Technol. Lett.*, vol. 15, no. 11, pp. 1612–1614, Nov. 2003.

[17] L.-S. Yan, M. C. Hauer, Y. Shi, X. S. Yao, P. Ebrahimi, Y. Wang, A. E. Willner, and W. L. Kath, "Polarization mode dispersion emulator using variable differential-group-delay elements and its use for experimental importance sampling," *J. Lightw. Technol.*, vol. 22, no. 4, pp. 1051–1058, Apr. 2004.

[18] C. K. Madsen *et al.*, "Versatile integrated PMD emulation and compensation elements," *J. Lightw. Technol.*, vol. 22, no. 4, pp. 1041–1050, Apr. 2004.

[19] Y. K. Lizé, L. Palmer, N. Godbout, S. Lacroix, and R. Kashyap, "Scalable polarization mode dispersion emulator with proper first and second order statistics," *IEEE Photon. Technol. Lett.*, vol. 17, no. 11, pp. 2451–2453, Nov. 2005.

[20] L. Moller *et al.*, "A tunable interferometrically stable three-section higher order PMD emulator," *IEEE Photon. Technol. Lett.*, vol. 15, no. 2, pp. 230–232, Feb. 2003.

[21] M. Wegmuller, S. Demma, C. Vinegoni, and N. Gisin, "Emulator of first- and second-order polarization-mode dispersion," *IEEE Photon. Technol. Lett.*, vol. 14, no. 5, pp. 630–632, May 2002.

[22] N. Y. Kim and N. K. Park, "Independently tunable first- and second-order polarization-mode dispersion emulator," *IEEE Photon. Technol. Lett.*, vol. 17, no. 3, pp. 576–578, Mar. 2005.

[23] P. B. Phua and H. A. Haus, "A deterministically controlled four-segment polarization-mode-dispersion emulator," *J. Lightw. Technol.*, vol. 20, no. 7, pp. 1132–1140, Jul. 2002.

[24] J. H. Lee, M. S. Kim, and Y. C. Chung, "Statistical PMD emulator using variable DGD elements," *IEEE Photon. Technol. Lett.*, vol. 15, no. 1, pp. 54–56, Jan. 2003.

[25] P. B. Phua, H. A. Haus, and E. P. Ippen, "Deterministic broad-band PMD emulator," *IEEE Photon. Technol. Lett.*, vol. 16, no. 6, pp. 1486–1488, Jun. 2004.

[26] L.-S. Yan, Y. Q. Shi, X. S. Yao, and A. E. Willner, "All-order PMD emulator with tunable statistics," in *Proc. LEOS Summer Top. Meeting*, Vancouver, BC, Canada, Jul. 15–17, 2003, pp. TuB3.2/43–TuB3.2/44.

[27] L.-S. Yan, C. Yeh, G. Yang, L. Lin, Z. Chen, Y. Q. Shi, A. E. Willner, and X. S. Yao, "Programmable group delay module using binary polarization switching," *J. Lightw. Technol.*, vol. 21, no. 7, pp. 1676–1684, Jul. 2003.

[28] P. B. Phua and H. A. Haus, "Variable differential-group-delay module without second-order PMD," *J. Lightw. Technol.*, vol. 20, no. 9, pp. 1788–1794, Sep. 2002.

[29] H. Bűlow, "Self-stabilizing continuously tunable group delay line for PMD compensation," presented at the Eur. Conf. Opt. Commun., Copenhagen, Denmark, 2002, Paper 9.3.5.

[30] Q. Yu, L.-S. Yan, S. Lee, Y. Xie, and A. E. Willner, "Loop-synchronous polarization scrambling technique for simulating polarization effects using recirculating fiber loops," *J. Lightw. Technol.*, vol. 21, no. 7, pp. 1593–1600, Jul. 2003.

[31] H. Xu, B. S. Marks, J. Zweck, L. Yan, C. R. Menyuk, and G. M. Carter, "Statistical properties of the DGD in a long-haul optical fiber system with temporally drifting birefringence," *J. Lightw. Technol.*, vol. 24, no. 3, pp. 1165–1175, Mar. 2006.

[32] C. H. Prola, Jr. *et al.*, "PMD emulators and signal distortion in 2.48-Gb/s IM-DD lightwave systems," *IEEE Photon. Technol. Lett.*, vol. 9, no. 6, pp. 842–844, Jun. 1997.

[33] J. Evans, "The birefringent filter," *J. Opt. Soc. Amer.*, vol. 39, no. 3, pp. 229–242, 1949.

[34] A. Galtarossa *et al.*, "Measurement of local beat length and differential group delay in installed single-mode fibers," *J. Lightw. Technol.*, vol. 18, no. 10, pp. 1389–1394, Oct. 2000.

[35] C. Antonelli and A. Mecozzi, "Statistics of the DGD in PMD emulators," *IEEE Photon. Technol. Lett.*, vol. 16, no. 8, pp. 1840–1842, Aug. 2004.

[36] G. Biondini, W. L. Kath, and C. R. Menyuk, "Importance sampling for polarization mode dispersion: Techniques and applications," *J. Lightw. Technol.*, vol. 22, no. 4, pp. 1201–1215, Apr. 2004.

[37] D. Yevick, "Multicanonical communication system modeling application to PMD statistics," *IEEE Photon. Technol. Lett.*, vol. 14, no. 11, pp. 1512–1514, Nov. 2002.

[38] L.-S. Yan, Q. Yu, and A. E. Willner, "Uniformly distributed states of polarization on the Poincaré sphere using an improved polarization scrambling scheme," *Opt. Commun.*, vol. 249, no. 1–3, pp. 43–50, May 2005.

[39] G. J. Foschini, L. E. Nelson, R. M. Jopson, and H. Kogelnik, "Probability densities of second-order polarization mode dispersion including polarization dependent chromatic fiber dispersion," *IEEE Photon. Technol. Lett.*, vol. 12, no. 3, pp. 293–295, Mar. 2000.

[40] L.-S. Yan *et al.*, "High-speed, stable and repeatable PMD emulator with tunable statistics," in *Proc. OFC*, Atlanta, GA, Mar. 2003, pp. 6–7.

[41] I. T. Lima, A. O. Lima, G. Biondini, C. R. Menyuk, and W. L. Kath, "A comparative study of single-section polarization-mode dispersion compensators," *J. Lightw. Technol.*, vol. 22, no. 4, pp. 1023–1032, Apr. 2004.

[42] G. Biondini and W. L. Kath, "Polarization mode dispersion emulation with Maxwellian lengths and importance sampling," *IEEE Photon. Technol. Lett.*, vol. 16, no. 3, pp. 789–791, Mar. 2004.

[43] T. Lu, D. Yevick, L.-S. Yan, B. Zhang, and A. E. Willner, "An experimental approach to multicanonical sampling," *IEEE Photon. Technol. Lett.*, vol. 16, no. 8, pp. 1978–1980, Aug. 2004.

[44] L.-S. Yan, T. Lu, B. Zhang, C. Yu, D. Yevick, and A. E. Willner, "Fiber transmission system application and limitation of multicanonical sampling in PMD emulation," presented at the Optical Fiber Commun. Conf., Anaheim, CA, 2005, Paper OThT4.

[45] M. Shtaif, "The Brownian-Bridge method for simulating polarization mode dispersion in optical communications systems," *IEEE Photon. Technol. Lett.*, vol. 15, no. 1, pp. 51–53, Jan. 2003.

[46] M. Brodsky, M. Boroditsky, P. Magill, N. J. Frigo, and M. Tur, "Persistence of spectral variations in DGD statistics," *Opt. Express*, vol. 13, no. 11, pp. 4090–4095, May 2005.

[47] M. Boroditsky, M. Brodsky, N. J. Frigo, P. Magill, C. Antonelli, and A. Mecozzi, "Outage probability for fiber routes with finite number of degrees of freedom," *IEEE Photon. Technol. Lett.*, vol. 17, no. 2, pp. 345–347, Feb. 2005.

[48] H. Kogelnik, P. J. Winzer, L. E. Nelson, R. M. Jopson, M. Boroditsky, and M. Brodsky, "First-order PMD outage for hinge model," *IEEE Photon. Technol. Lett.*, vol. 17, no. 6, pp. 1208–1210, Jun. 2005.

[49] L.-S. Yan, X. S. Yao, and A. E. Willner, "Enabling hinge model in polarization-mode-dispersion statistics using variable differential-group-delay based emulator," *IEEE Photon. Technol. Lett.*, vol. 18, no. 2, pp. 427–429, Jan. 2006.
[50] C. Xie and H. Haunstein, "Optimum length of one-stage polarization-mode-dispersion compensators with a fixed delay line," *IEEE Photon. Technol. Lett.*, vol. 15, no. 9, pp. 1228–1230, Sep. 2003.
[51] Q. Yu and A. E. Willner, "Performance limits of first-order PMD compensators using fixed and variable DGD elements," *IEEE Photon. Technol. Lett.*, vol. 14, no. 3, pp. 304–306, Mar. 2002.
[52] S. Kieckbusch, S. Ferber, H. Rosenfeldt, R. Ludwig, C. Boerner, A. Ehrhardt, E. Brinkmeyer, and H.-G. Weber, "Automatic PMD compensator in a 160-G/s OTDM transmission over deployed fiber using RZ-DPSK modulation format," *J. Lightw. Technol.*, vol. 23, no. 1, pp. 165–171, Jan. 2005.
[53] L.-S. Yan, Q. Yu, A. B. Sahin, and A. E. Willner, "Differential group delay monitoring used as feed forward information for polarization mode dispersion compensation," *IEEE Photon. Technol. Lett.*, vol. 14, no. 10, pp. 1463–1465, Oct. 2002.
[54] Q. Yu, L.-S. Yan, Y. Xie, M. Hauer, and A. E. Willner, "Higher-order PMD compensation using a fixed time delay followed by a variable time delay," *IEEE Photon. Technol. Lett.*, vol. 13, no. 8, pp. 863–865, Aug. 2001.
[55] F. Heismann, "Improved optical compensator for first- and second-order polarization-mode dispersion," *IEEE Photon. Technol. Lett.*, vol. 17, no. 5, pp. 1016–1018, May 2005.
[56] H. Sunnerud, C. Xie, M. Karlsson, R. Samuelsson, and P. A. Andrekson, "A comparison between different PMD compensation techniques," *J. Lightw. Technol.*, vol. 20, no. 3, pp. 368–378, Mar. 2002.
[57] G. Lorenzetto, A. Galtarossa, L. Palmieri, M. Santagiustina, C. G. Someda, and R. Fiorone, "Analysis of feedback for higher order polarization-mode dispersion mitigation of NRZ 40-Gb/s optical transmission," *J. Lightw. Technol.*, vol. 21, no. 2, pp. 424–431, Feb. 2003.
[58] L.-S. Yan, Q. Yu, T. Luo, A. E. Willner, and X. S. Yao, "Compensation of higher-order PMD using phase modulation and polarization control in the transmitter," *IEEE Photon. Technol. Lett.*, vol. 14, no. 6, pp. 858–860, Jun. 2002.
[59] P. C. Chou, J. M. Fini, and H. A. Haus, "Real-time principal state characterization for use in PMD compensators," *IEEE Photon. Technol. Lett.*, vol. 13, no. 6, pp. 568–570, Jun. 2001.
[60] X. Zhang, Y. Zheng, Y. Shen, J. Zhang, and B. Yang, "Particle swarm optimization used as a control algorithm for adaptive PMD compensation," *IEEE Photon. Technol. Lett.*, vol. 17, no. 1, pp. 85–87, Jan. 2005.
[61] C. Xie and L. Moller, "Comparison of different feedback signals for one-stage polarization-mode-dispersion compensators," *IEEE Photon. Technol. Lett.*, vol. 17, no. 3, pp. 570–572, Mar. 2005.
[62] A. E. Willner, S. M. R. Motaghian Nezam, L.-S. Yan, Z. Pan, and M. C. Hauer, "Polarization monitoring and control in optical systems," *J. Lightw. Technol.*, vol. 22, no. 1, pp. 106–125, 2004.
[63] R. Noé, D. Sandel, and V. Mirvoda, "PMD in high-bit-rate transmission and means for its mitigation," *IEEE J. Sel. Topics Quantum Electron.*, vol. 10, no. 2, pp. 341–355, Mar./Apr. 2004.
[64] S. Lanne and E. Corbel, "Practical considerations for optical polarization-mode dispersion compensators," *J. Lightw. Technol.*, vol. 22, no. 4, pp. 1033–1040, Apr. 2004.
[65] C. Xie, L. Moller, H. Haunstein, and S. Hunsche, "Comparison of system tolerance to polarization-mode-dispersion between different modulation formats," *IEEE Photon. Technol. Lett.*, vol. 15, no. 8, pp. 1168–1170, Aug. 2003.
[66] C. R. Doerr, S. Chandrasekhar, P. J. Winzer, A. R. Chraplyvy, A. H. Gnauk, L. W. Stulz, R. Pafchek, and E. Burrows, "Simple multichannel optical equalizer mitigating intersymbol interference for 40-Gb/s nonreturn-to-zero signals," *J. Lightw. Technol.*, vol. 22, no. 1, pp. 249–256, Jan. 2004.
[67] F. Buchali and H. Bulow, "Adaptive PMD compensation by electrical and optical techniques," *J. Lightw. Technol.*, vol. 22, no. 4, pp. 1116–1126, Apr. 2004.
[68] M. Akbbulut, A. M. Weiner, and P. J. Miller, "Broadband all-order polarization mode dispersion compensation using liquid-crystal modulator arrays," *J. Lightw. Technol.*, vol. 24, no. 1, pp. 251–261, Jan. 2006.
[69] C. Antonelli, A. Mecozzi, and M. Boroditsky, "Broad-band PMD mitigation with a single polarization controller," *IEEE Photon. Technol. Lett.*, vol. 17, no. 12, pp. 2574–2576, Dec. 2005.
[70] X. Liu, C. R. Giles, X. Wei, A. J. van Wijingaarden, Y.-H. Kao, C. Xie, L. Moller, and I. Kang, "Demonstration of broad-band PMD mitigation in the presence of PDL through distributed fast polarization scrambling and forward-error correction," *IEEE Photon. Technol. Lett.*, vol. 17, no. 5, pp. 1109–1111, May 2005.
[71] A. Eyal and A. Yariv, "Design of broad-band PMD compensation filters," *IEEE Photon. Technol. Lett.*, vol. 14, no. 8, pp. 1088–1090, Aug. 2002.
[72] B. Huttner, C. Geiser, and N. Gisin, "Polarization-induced distortions in optical fiber networks with polarization-mode dispersion and polarization-dependent losses," *IEEE J. Sel. Topics Quantum Electron.*, vol. 6, no. 2, pp. 317–329, Mar./Apr. 2000.
[73] L.-S. Yan, Q. Yu, Y. Xie, and A. E. Willner, "Experimental demonstration of the system performance degradation due to the combined effect of polarization dependent loss with polarization mode dispersion," *IEEE Photon. Technol. Lett.*, vol. 14, no. 2, pp. 224–226, Feb. 2002.
[74] W. Shieh and S. D. Dods, "Robustness of polarization-mode-dispersion compensation in the presence of polarization-dependent loss," *IEEE Photon. Technol. Lett.*, vol. 17, no. 3, pp. 573–575, Mar. 2005.
[75] G. Zhang, J. T. Stango, X. Zhang, and C. Xie, "Impact of fiber nonlinearity on PMD penalty in DWDM transmission systems," *IEEE Photon. Technol. Lett.*, vol. 17, no. 2, pp. 501–503, Feb. 2005.

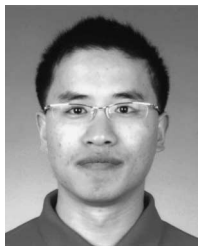

Lianshan Yan (S'99–M'05–SM'06) received the B.E. degree in optical engineering from Zhejiang University, Hangzhou, China, in 1994 and the Ph.D. degree in electrical engineering from the University of Southern California (USC), Los Angeles, in 2005.

From 1994 to 1999, he was with North China Research Institute of Electro-optics, where he worked on solid-state lasers. In September 1999, he joined the Optical Communications Laboratory, USC. He is currently a Senior Scientist and the Manager of engineering with General Photonics Corporation, Chino, CA, concentrating on polarization, timing, and spectrum control. He is the author and a coauthor of more than 100 papers in prestigious journals and conference proceedings. He is the holder of four U.S. patents and about ten pending ones. His research interests include enabling technologies for long-haul wavelength-division-multiplexing systems and polarization effects in fiber transmission.

Dr. Yan was a recipient of the IEEE Lasers and Electro-Optic Society (LEOS) Graduate Fellowship in 2002. He serves as a frequent referee for ten journals. He is a Senior Member of the IEEE LEOS and a member of the Optical Society of America and the Sigma Xi society.

X. Steve Yao (M'97) received the M.S. and Ph.D. degrees in electrical engineering/electrophysics from the University of Southern California, Los Angeles, in 1989 and in 1992, respectively.

From 1985 to 1987, he was an Optical Engineer with ADC Fiber Optics (a division of ADC Telecommunications), where he developed the first generation of fiber-optic wavelength-division-multiplexing devices. From 1990 to 2000, he was with the Jet Propulsion Laboratory, NASA, Pasadena, CA, where he worked on research and development of microwave photonic devices and systems and invented the optoelectronic oscillator that generates the world's cleanest 10–80-GHz signals. He was responsible for the design and demonstration of the X-band fiber-optic antenna remoting system for NASA's Deep Space Network. He is currently the Chief Technology Officer with General Photonics Corporation, Chino, CA, which is a company that provides the most complete product selections for polarization and timing control for the telecommunications and sensor industry. He is the author of more than 40 referred journal publications and a book chapter in *RF Photonic Technology in Optical Fiber Links* (Cambridge Univ. Press, 2002), which details his breakthrough research in an optoelectronic oscillator for generating 10-GHz and higher frequency signals. He has given invited speeches in numerous major photonics-related conferences and holds more than 30 issued U.S. patents and 15 pending applications.

Dr. Yao is a recipient of 29 innovation awards from NASA. Two products based on his inventions have won the Photonics Circle of Excellence Awards in 2000 and 2001, respectively. The awards are given to the top 25 most innovative products around the world each year. He also served as a member of the Technical Committee of the Optical Fiber Communications conferences and was an organization committee member for the Microwave Photonics Conference in 2000.

M. C. Hauer (S'04), photograph and biography not available at time of publication.

A. E. Willner (S'87–M'88–SM'93–F'04), photograph and biography not available at time of publication.